Nucleolin targeting impairs the progression of pancreatic cancer and promotes the normalization of tumor vasculature

Maud-Emmanuelle Gilles, Federica Maione, Mélissande Cossutta, Gilles Carpentier, Laure Caruana, Silvia Di Maria, Claire Houppe, Damien Destouches, Ksenya Shchors, Christopher Prochasson, Fabien Mongelard, Simona Lamba, Alberto Bardelli, Philippe Bouvet, Anne Couvelard, José Courty, Enrico Giraudo, Ilaria Cascone

Paper: Nucleolin Targeting Impairs the Progression of Pancreatic Cancer and Promotes the Normalization of Tumor Vasculature

CANCER RESEARCH, 76 (24), 2016, pp: 7181-7193

DOI: 10.1158/0008-5472.CAN-16-0300

Nucleolin targeting impairs the progression of pancreatic cancer and promotes the normalization of tumor vasculature

Maud-Emmanuelle Gilles[1§], Federica Maione[2§], Mélissande Cossutta[1§], Gilles Carpentier[1], Laure Caruana[1], Silvia Di Maria[1], Claire Houppe[1], Damien Destouches[1], Ksenya Shchors[3], Christopher Prochasson[4], Fabien Mongelard[5], Simona Lamba[6], Alberto Bardelli[6,7], Philippe Bouvet[5], Anne Couvelard[4], José Courty[1]*, Enrico Giraudo[2]* and Ilaria Cascone[1]*

[1] Université Paris-Est, UPEC, CNRS, ERL 9215, Laboratoire de Recherche sur la Croissance Cellulaire, la Réparation et la Régénération Tissulaires (CRRET), F-94000 Créteil, France.
[2] Laboratory of Transgenic Mouse Models, Candiolo Cancer Institute, FPO-IRCCS, and Department of Science and Drug Technology, University of Torino, Italy.
[3] Swiss Institute for Experimental Cancer Research (ISREC), EPFL SV ISREC, Station 19, CH-1015 Lausanne.
[4] Département de Pathologie, Hôpital Bichat APHP DHU UNITY, Paris, France.
[5] Université de Lyon, Ecole normale Supérieure de Lyon, Centre de Recherche en Cancérologie de Lyon, Cancer Cell Plasticity Department, UMR INSERM 1052 CNRS 5286, Centre Léon Bérard, Lyon, France.
[6] Department of Oncology, University of Torino, SP 142 km 3.95, 10060 Candiolo (TO), Italy.
[7] Candiolo Cancer Institute-FPO, IRCCS, 10060 Candiolo (TO), Italy.

The authors have not conflict of interest

[§] co-authorship
*co-seniorship

Correspondence should be addressed to:

Ilaria Cascone, PhD,
Université Paris Est Créteil Val de Marne
61 avenue du Général de Gaulle
94010 Créteil Cedex
Phone: +330145171799
E-mail: ilaria.cascone@u-pec.fr

Enrico Giraudo, PhD
Department of Science and Drug Technology, University of Torino,
and Laboratory of Transgenic Mouse Models,
Candiolo Cancer Institute – FPO, IRCCS
Strada Provinciale 142, Km 3.95
I-10060 Candiolo, Turin, Italy
Phone: +390119933505
E-mail: enrico.giraudo@ircc.it

Running title: Nucleolin targeting impairs pancreatic cancer

Keywords: Pancreatic cancer, anti-angiogenic therapy, nucleolin, angiogenesis, vessel normalization, Ang-2

ABSTRACT

Pancreatic cancer is a highly aggressive tumor, mostly resistant to the standard treatments. Nucleolin (NCL) is overexpressed in cancers and its inhibition impairs tumor growth. Herein we showed that NCL was overexpressed in human specimens of pancreatic ductal adenocarcinoma (PDAC) and that the overall survival significantly increased in patients with low levels of NCL. The NCL antagonist N6L strongly impaired the growth of primary tumors and liver metastasis in an orthotopic mouse model of PDAC (mPDAC). Similar anti-tumor effect of N6L has been observed in a highly angiogenic mouse model of pancreatic neuroendocrine tumor RIP-Tag2. N6L significantly inhibited both human and mouse pancreatic cell proliferation and invasion. Notably, the analysis of tumor vasculature revealed a strong increase of pericyte coverage and vessel perfusion both in mPDAC and RIP-Tag2 tumors, in parallel to an inhibition of tumor hypoxia. NCL inhibition directly affected endothelial cell (EC) activation and changed a pro-angiogenic signature. Among the vascular activators, NCL inhibition significantly decreased Ang-2 secretion and expression in ECs, in the tumor and in the plasma of mPDAC mice. As a consequence of the observed N6L-induced tumor vessel normalization, pre-treatment with N6L efficiently improved chemotherapeutic drug delivery and increased the anti-tumor properties of gemcitabine in PDAC mice.

In conclusion, NCL inhibition is a new anti-pancreatic cancer therapeutic strategy that dually blocks tumor progression and normalizes tumor vasculature improving the delivery and efficacy of chemotherapeutic drugs. Moreover, we unveiled Ang-2 as a potential target and suitable response biomarker for N6L treatment in pancreatic cancer.

INTRODUCTION

Pancreatic cancer which include Pancreatic Ductal Adenocarcinoma (PDAC) and Pancreatic neuroendocrine tumors (PNETs) is the fourth most common cause of cancer deaths worldwide (1). PDAC is a highly aggressive cancer with a very poor prognosis and an overall 5-year survival rate less than 5%. Current therapies in PDAC and PNET, consist solely of surgery followed or not by targeted or chemo therapies (2, 3).

Nucleolin (NCL) is highly expressed in several types of cancer (4), and is a cancer specific target, being localized at the cell surface of tumor cells and activated endothelial cells (ECs) (5-7). Nucleolar NCL principally regulates rRNA transcription and ribogenesis while cell surface NCL acts as a low affinity receptor for specific ligands (4). Moreover, NCL stabilizes the mRNA of anti-apoptotic proteins (8). NCL is a novel target for anticancer therapy as demonstrated by the effects of several NCL-targeting molecules (9-11). We recently developed a multivalent synthetic pseudopeptide N6L that selectively binds to NCL (9). N6L strongly inhibits breast cancer growth by inducing apoptosis of tumor cells and is currently in preparation for phase II clinical trials (9) (IPP-204106). Interestingly, N6L as well as a NCL blocking antibody impairs both experimental and *in vivo* angiogenesis by targeting endothelial cells and tumor vessels (9, 12, 13). The mechanisms of regulation of tumor angiogenesis by NCL are poorly described, such as the effect of NCL inhibition in tumor cells and stroma of pancreatic cancer.

Several molecules that regulate tumor angiogenesis are overexpressed in pancreatic cancer. In human PDAC, VEGF expression is increased and high levels of Ang-2 correlate with metastatic spread and poor survival of PDAC patients (14, 15). However, blood vessels in PDAC are compressed by the fibrous stroma and PDAC is poorly perfused with a consequent aberration in local blood flow and oxygenation (16). This contributes to the promotion of cancer growth, tumor hypoxia, metastasis formation and prevents an efficient delivery of

chemotherapeutic drugs (17, 18). PNETs, differently from PDAC are highly vascularized, but share the same vascular abnormality phenotype that contributes to cancer progression and metastatic dissemination (3).

Based on these findings our aim was to target both cancer cells and tumor vasculature in pancreatic cancer. In this work, we studied NCL-targeted therapy, demonstrating that N6L, hampers pancreatic cancer growth and metastasis by dually targeting cancer cell growth and tumor vasculature, and we explored the potential mechanisms of action.

MATERIALS AND METHODS

The source of antibodies (Abs) and the experimental procedures not described herein are detailed in Supplementary Data.

Cell culture

Human umbilical vein endothelial cells (HUVECs) were authenticated by Lonza and periodically provided between 2013-2015, cultured in EGM-2 and used until the fourth passage. Human Brain Vascular Pericytes (HBVP) were authenticated and provided by ScienCell in 2014, maintained in Pericyte Medium phenol red free (PM-prf, ScienCell) containing appropriated growth supplements and used until the fourth passage. Murine pancreatic cancer cell (mPDAC), were isolated, as described in Supplementary methods, from tumor-bearing $p48^{cre}$, $Kras^{LSL\_G12D}$, $p53^{R172H/+}$, $Ink4a/Arf^{flox/+}$ mice in 2012 and the genotype was verified by PCR.

Tumor mouse models

FVB/n syngenic mice were injected orthotopically in the pancreas with mPDAC cells (10^3 cells/mouse in 50 μL). In this mPDAC model, we first established that the tumors reach a

volume of approximately 80 mm^3 within a week following injection of tumor cells. We defined this time period as the starting point to perform a regression trial, and one week after cell inoculation, mice were treated 3 times a week for the duration of 3 weeks by intraperitoneal injections (i.p.) with either N6L (10 mg/kg) or vehicle (saline solution) as a control. Gemcitabine was injected in the tail vein (i.v.) (100 mg/kg) 2 times a week as indicated. In the combination treatment, GEM was injected 2 times (i.v.) a week and N6L 3 times a week (i.p.) after 1 week of N6L for a total of 2 weeks to the animals. Regarding the measurement of metastasis, livers from PDAC mice were entirely cut and sections spaced of 200 μm were stained by hematoxylin. Images were taken by Scanner Aperio Scanscope CS. The metastatic surface of each nodule in the liver sections was measured, and the total surface occupied by metastasis was divided by the total area of the liver section.

The RIP-Tag2 transgenic mouse model has been previously described (19), mice were treated by N6L 10 mg/kg, 3 times a week for a duration of 4 weeks from 12 to 16 weeks of age.

Mice were sacrified and total tumor burden was quantified as previously described (9). All *in vivo* experiments were carried out with the approval of the appropriate ethical committee and under conditions established by the European Union.

TMA staining and analysis

An immunohistochemical staining was performed with anti-nucleolin antibody (Supplementary methods) using standard protocol in 47 human PDAC included in a tissue-microarray (TMA) paraffin block. Immunostaining was performed using an automatized technique (Streptavidin-peroxydase with an automate Bond Max, Leica), and slides were counterstained with hematoxylin. Images were taken by the Scanner Aperio Scanscope CS. Analysis of NCL staining was performed by a score determination corresponding to the intensity of the labeling of tumor cells from 0 to 3 (0, no staining; 1, low staining; 2, moderate

staining; 3, high staining) in each spot. The final score for each tumor was the average of the scores obtained for each spot available by tumor.

Measurement of tumor delivery of doxorubicin and vessel perfusion

To evaluate tumor vessel perfusion, 0.05 mg FITC-labeled tomato lectin (Vector laboratories, CA, USA) were injected i.v. into PDAC-carrying mice, as previously described (20). After 10 minutes, the animals were euthanized, and lectin distribution was visualised by fluorescent confocal microscopy.

To measure the tumor delivery of doxorubicin mice were injected with 10 mg/kg doxorubicin hydrochloride (Sigma-Aldrich) *via* the lateral tail vein 4 hours before sacrifice. Tumors and kidneys as controls were collected from each mouse and weighted. Samples were resuspended in a lysis buffer (0.25 M sucrose, 5 mM TrisHCl pH 7.6, 1 mM $MgSO_4$, 1 mM $CaCl_2$) and homogenized in an ice-cold Potter homogenizer. 200 µl of each homogenate was placed into a new microcentrifuge tube containing 10% Triton X-100 and 1.5 ml acidified isopropanol, mixed and kept at –20°C overnight. Samples were centrifuge at 15,000 *g* for 20 minutes. Doxorubicin was quantified by spectrophotometric analysis at 590 nm using TECAN Infinite M1000 plate reader (Tecan, Durham, NC). These values were calculated as the fluorescence/weight ratio of the tumor divided by the fluorescence/weight ratio of the kidney and expressed as µ equivalents/g tissue of doxorubicin. Data are mean ± SD of triplicate aliquots from tumor homogenates.

Cell transfection and cell migration

Cell transfection by siRNA was performed by following manufacturer instructions (Hiperfect, Qiagen), for siRNA sequences see Supplementary methods.

For pericyte motility, $9x10^4$ HUVECs per well were seeded in 6-well plate. The day after, HUVECs were transfected with 10 nM siRNA or treated with 30 μM N6L. Three days later HUVECs were washed and medium was replaced by EBM-2. Cell supernatant was collected 1 hour after. $20x10^4$ HBVPs were seeded in the upper chamber (with or without 400 ng/mL recombinant Ang2) coated with 1.5 ug/mL collagen type I and the EC supernatant was added in the lower chamber. For each transwell, nuclei of cells from 5 fields were counted using Leica Aristoplan microscope equipped with a CoolSNAP CCD camera.

Statistics

Unless indicated otherwise, bars represent mean +/− Standard Error Mean (S.E.M.) ($n \geq 3$), p-values have been calculated using a two-tailed or one-tailed unpaired t test using GraphPad Prism software. *$p < 0.05$; **$p < 0.01$; ***$p < 0.001$; ****$p<0.00001$. P values of the Kaplan-Meier curve of survival has been calculated by using the Long-rank (Mantel-Cox) test.

RESULTS

NCL is a potential new target of tumor progression in PDAC.

NCL is overexpressed in tumors and its inhibition hampers breast, prostate, and melanoma cancer growth and angiogenesis (4). To evaluate NCL as a potential target in human PDAC, we analyzed NCL protein expression levels in 47 tumors included in tissue microarray. 74.5% of the tumors showed a moderate (Fig. 1C) or high NCL staining (Fig. 1A and, B arrows). Non-tumoral pancreas, corresponding to pancreatitis (Fig. 1D), normal peritumoral tissue or normal ducts either around or included in the tumors (Fig. 1B, arrowheads) were not or very faintly stained by anti-NCL antibody. Next, we checked the correlation between NCL expression level and overall survival (OS) in patients with PDAC. Notably, the OS significantly increased in PDAC patients with low levels of NCL compared to patients with high levels of this protein (Fig. 1E).

NCL protein level was analyzed in four different human pancreatic cancer cell lines (hPDAC), a murine PDAC cell line (mPDAC) and endothelial cells (ECs) (Supplementary Fig. 1A). Capan-2 and BxPC-3 showed similar protein level than non tumoral cells, ECs, while MIA PaCa-2, PANC-1 and mPDAC cell lines displayed higher NCL protein levels. We sought to investigate whether NCL inhibition affects progression of PDAC. The multivalent pseudopeptide N6L (9) bound to NCL in human pancreatic cancer cells PANC-1, as well as in ECs (Supplementary Fig. 1B). N6L inhibited pancreatic cell growth of all cell lines cited above (Supplementary Fig. 1C). The GI_{50} is in a range between 5 to 36 μM and increased with NCL levels, by a. Coherently, N6L significantly reduced the amount of PDAC cells in S phase after 24 hours of treatment (Supplementary Fig 1D), and the active caspase-3 levels increased after 48 hours of treatment (Supplementary Fig. 1E). Moreover, N6L strongly inhibited the migration of MIA PaCa2 and mPDAC cell lines by 69% and 72%, respectively, compared with controls (Supplementary Fig. 1F), and the invasion of mPDAC cells toward a

layer of matrigel, as compared to controls (Supplementary Fig. 1G). The implication of NCL in PDAC cell proliferation was tested by other experimental approaches. For instance, the viability of mPDAC cells was decreased by a NCL blocking antibody (MS3) (Supplementary Fig. 2A). Moreover, the knock down of *Ncl* in mPDAC by means of CRISP-Cas9 technology caused massive death of the cells (Supplementary Fig. 2C). NCL blocking antibody pre-treatment decreased the efficacy of the entry of Alexa546-N6L in PDAC cells (Supplementary Fig. 2B). In line with these results, the combination of NCL blocking antibody and N6L did not show a cumulative effect on cell viability (Supplementary Fig. 2A). These results suggested that N6L and NCL blocking antibody competed for NCL targeting in PDAC cells.

N6L treatment hampers PDAC growth and liver metastasis.

Based on the high levels of NCL found in human PDAC, and according to the observation that N6L inhibited hPDAC and mPDAC cell proliferation, we decided to assess the anti-tumor effect of N6L in an orthotopic mouse model of PDAC. The model was obtained by injecting mPDAC tumor cells orthotopically into the pancreas of a cohort of FVB/n syngenic mice (from here the model will be called mPDAC model). This model recapitulated many features of the human PDAC, showing a malignant epithelial neoplasm with ductal differentiation (Supplementary Fig. 3A) or sarcomatoid carcinoma (Supplementary Fig. 3B) (21). Tumor tissues in mPDAC model were highly hypoxic (Supplementary Fig. 3C) and fibrotic (Supplementary Fig. 3E, arrows), and showed a high heterogeneity of vessel density as in human patients (22), with poorly vascularized regions (arrows in Supplementary Fig. 3D) and regions with a higher vessel density (arrowheads in Supplementary Fig. 3D). Notably, carbonic anhydrase 9 (CA9) expression significantly increased in parallel with enhanced synthesis of collagen I during cancer progression in mPDAC (Supplementary

Figure 3E, F and G). These data suggest that, similarly to the human disease, hypoxic level well correlated with increased fibrosis in PDAC tumors. Similarly to human samples (Fig. 1 A-D), NCL was expressed in the nuclei of pancreatic acinar cells (Supplementary Fig 3K) but highly expressed in tumor tissues compared to healthy pancreas (Supplementary Fig. 3H, I, K and L), in particular in ducts and sarcomatoid regions of the tumor (Supplementary Fig. 3H and I). In addition, NCL was significantly expressed in the tumor vasculature of mPDAC model (Supplementary Fig. 3J).

The treatment of mPDAC mice with 10 mg/kg of N6L significantly decreased the tumor volume by 43.4% (Fig. 2A). The rate of proliferative cells decreased in PDAC tumors treated by N6L compared with controls (Fig. 2B and C) while, N6L treatment enhanced apoptosis in tumor cells (Fig. 2B and D). Since NCL expression is coupled to tumor cell proliferation (6), we analyzed the effect of N6L on NCL protein (Fig 2B and E) and mRNA levels of tumors (Fig. 2F). Consistently, both NCL mRNA and protein were decreased in N6L-treated mPDAC (Fig. 2B, E and F).

Two ways of dissemination to the liver are described in PDAC patients, through vessels and through a peritoneal dissemination. mPDAC model developed liver metastasis prominently in the liver at close contact to the peritoneal surface (Fig. 2G, arrows). The total metastatic area was quantified (Fig. 2H). Remarkably, N6L strongly reduced liver metastasis area by 67% (Fig. 2G and H). These findings are further supported by our data describing a strong effect of N6L in blocking the motility and the invasion of mouse and tumor cell lines (Supplementary Fig. 1F and G).

NCL targeting by N6L normalizes tumor vessels and counteracts tumor hypoxia in PDAC and PNET.

Since NCL targeting inhibits EC growth and NCL is significantly expressed in the vasculature

of mPDAC, we investigated the effect of N6L on tumor blood vessel density and morphology. Vessel density and vessel branching were significantly decreased in N6L-treated mPDAC by 42% and by 62%, respectively (Fig. 3A, B and C). Therefore, the effect of N6L on tumor vessel normalization in mPDAC tumors was studied by analyzing the changes in pericyte vessel coverage, perfusion, and hypoxic levels, all hallmarks of vessel normalization in cancer (23). In mPDAC model, tumor blood vessels typically had low pericyte coverage, detected with two different markers of pericytes (24). The treatment of mPDAC tumors with N6L 10 mg/kg resulted in an increase of pericyte coverage of tumor blood vessels. $NG2^+$ pericytes increased by 71% (Fig. 3A and D) and PDGFR-β^+ pericytes by 77% of (Fig. 3A, and E). The treatment with N6L 2 mg/kg resulted in an increase of $NG2^+$ pericyte coverage of tumor blood vessel by 52% (Supplementary Fig. 4A), supporting a dose effect of N6L. Then, we sought to evaluate the effect of the inhibition of stromal NCL *vs* tumoral cell NCL on tumor vascularization. We evaluated the tumor vascularization and pericyte coverage in an orthotopic mouse model of pancreatic tumor generated by injecting PDAC cells (Panc-02) into the pancreas of wild type ($Ncl^{wt/wt};Cre^{+/-}$) mice or in animals in which NCL was deleted in one allele ($Ncl^{flwt};Cre^{+/-}$) (Supplementary Fig. 4B and C). Remarkably, we observed reduced tumor vascularization (Supplementary Fig. 4D and E) and increased pericyte coverage in $Ncl^{+/-}$ (Supplementary Fig. 4F and G), compared with $Ncl^{+/+}$ mice.

Blood vessel perfusion is a parameter of vessel homeostasis and correlates with pericyte coverage and oxygenation (25). Interestingly, the treatment of mPDAC with N6L enhanced the perfusion of the tumor vasculature, compared with controls (Fig. 3F and G). Next, we assessed whether the tumor oxygenation levels were affected by N6L. In line with its normalizing effect, N6L reduced the hypoxic area, detected by pimonidazole staining (Fig. 3H). In addition, N6L strongly inhibited the expression of carbonic anhydrase 9 (CA9), a marker of hypoxia (26) (Fig. 3I and J).

To better assess the effects of N6L on tumor vessel normalization and the related anti-tumor properties, we employed a transgenic mouse model of pancreatic neuroendocrine tumor (PNET) RIP-Tag2. This model has been widely used to assess the efficacy of several anti-angiogenic compounds and to evaluate the effect of vessel normalization to block tumor growth and invasion (19, 24). To this aim, we performed a regression trial (24), treating a cohort of tumor-bearing RIP-Tag2 mice with N6L. This treatment showed an inhibition of tumor growth by 40% (Fig. 4A) and an increase of tumor cell apoptosis by 90% (Fig. 4B), compared with controls. Similarly to PDAC, N6L significantly induced tumor vessel normalization by increasing pericyte coverage (by 42%) (Fig. 4C and F), and enhanced the perfusion of the tumor vasculature (Fig. 4G and H). In line with these vessel normalization effects N6L-treated tumors showed reduced vessel number and branching (Fig. 4C, D and E). All together these results demonstrate that the inhibition of NCL induces vessel normalization in two different mouse models of pancreatic cancer by increasing pericyte coverage, vessel perfusion and reducing intra-tumoral hypoxia.

NCL inhibition affects EC activation and Ang-2 secretion.

The mechanisms of tumor inhibition and vessel normalization by N6L were further studied. N6L does not induce apoptosis of ECs (15), and did not change the viability value of confluent ECs (Supplementary Fig. 5A), suggesting that NCL inhibition specifically target proliferating and activated ECs. N6L significantly decreased the percentage of ECs in S phase when compared to control-treated cells (14% *vs* 27%) and increased the percentage of cells in G1 (64% *vs* 47%) (Fig. 5A). The involvement of NCL in EC cycle progression was further confirmed by depleting NCL in ECs. In fact, NCL depletion by siRNA significantly decreased the percentage of ECs in S phase, and increased the amount of cells in G1 phase when compared to control ECs (4% *vs* 32% and 86% *vs* 42%, respectively) (Fig. 5B).

Another feature of EC activation is the secretion of pro-angiogenic molecules by ECs (27). Therefore, we evaluated the effect of N6L on the basal secretion of angiogenic-related molecules by ECs by using a proteome angiogenesis antibody array (R&D). Interestingly, among the different secreted pro-angiogenic factors, we observed that Ang-2, shown to promote tumor progression and whose inhibition induces vessel normalization (28-32), was inhibited by N6L treatment (Supplementary Table 1). Based on this screening we analyzed the effect of N6L on the secretion of Ang-2 by ECs. Ang-2 level decreased in the EC supernatant upon 5 hours of N6L treatment but not in EC lysates (Fig. 5C). Ang-2 is stocked in Weibel and Palade bodies (WPBs) and basally secreted by WPB exocytosis in activated ECs (33). Ang-2 colocalized with the WPB protein vWF in ECs (Fig. 5D, inset). Interestingly, 5 hours of N6L treatment enhanced Ang-2 content (Fig 5D and E), indicating that N6L interferes with the turnover of Ang-2 secretion, accumulating this protein into ECs. The importance of NCL in Ang-2 secretion inhibition under N6L was tested (Fig 5F). While significant inhibition of secreted Ang-2 has been observed in siControl ECs treated with N6L, no detectable differences in Ang-2 levels were measured in siNCL-EC supernatants, compared with their respective controls (Fig. 5F). The effect of longer N6L treatment (72 hours) on Ang-2 expression was analyzed (Fig 5H an I). Ang-2 level decreased in EC lysates at the protein level (Fig 5H) and at the mRNA level (Fig 5I) under N6L treatment. Coherently, Ang-2 basal secreted levels (Fig. 5F) and Ang-2 protein level in ECs (Fig. 5G) were also decreased in NCL-depleted cells. These data suggest that NCL inhibition affects Ang-2 secretion and expression. In line with the observed pro-normalizing effect of N6L, among angiogenic-related secreted molecules in ECs, we observed that PDGFβ, a factor mediating pericyte recruitment (34), was also upregulated by N6L, (Supplementary Table 1) and its mRNA was significantly increased under N6L treatment (Supplementary Fig. 5B).

Together these data demonstrate that NCL depletion or inhibition by N6L affects EC activation by decreasing the percentage of cells in S phase and regulating angiogenic molecules involved in pericyte recruitment.

NCL inhibition decreases plasma Ang-2 level in PDAC model.

In human cancers Ang-2 is highly expressed by ECs in tumor blood vessels and tumor cells (35, 36). Notably, Ang-2 is expressed mostly in tumor blood vessel of PDAC model (Supplementary Fig 5D). Pilot studies aimed to measure the time-course of plasmatic Ang-2 amount showed that the levels of Ang-2 in the plasma were unchanged until the second week of PDAC growth and increased then after (Supplementary Fig 5E). Based on these preliminary data, we next analyzed plasmatic Ang-2 level of different mice injected by PDAC cells or saline solution after three weeks of inoculation (Fig 6A). As expected from our previous observation, Ang-2 was significantly increased in tumor bearing mice (Fig. 6A). To evaluate the effect of N6L-treatment on secreted Ang-2 levels *in vivo*, we checked the plasma of control and N6L-treated mPDAC at the end of the treatment. Remarkably, Ang-2 was significantly decreased by 68% in the plasma of N6L-treated mice compared with control (Fig. 6B), while PDGFβ level did not change (Supplementary Fig. 5G). In parallel, Ang-2 expression was evaluated in tumors. Since tumor vessel density was decreased in N6L-treated mPDAC (Fig. 3A and B), Ang-2 expression was normalized to the tumor vessel gene MECA32 and Fig 6C shows that Ang-2 expression decreased under N6L treatment. Notably, VEGF signaling was not affected by N6L, since VEGF-A expression (Supplementary Fig. 5F) was unchanged in N6L-treated PDAC tumors, and VEGFR2 levels was not affected in N6L-treated ECs (Supplementary Fig. 5C).

To better assess the role of secreted Ang-2 in vessel normalization, we sought to investigate whether decreased Ang-2 secretion by Ang-2-depleted or N6L-treated ECs was sufficient to

induce pericyte recruitment. Pericyte migration toward the supernatants of Ang-2-depleted ECs was strongly increased compared with control (Fig. 6D). Moreover, pericyte migration towards the supernatant of ECs treated with N6L was similarly increased (Fig 6E). Since pericytes express the Ang-2 receptor Tie-2 and Ang-2 induces dose-dependent pericyte loss on retina vessels (37), we investigated if Ang-2 could directly affect pericyte migration. Ang-2 functions are dependent to the context of angiogenic cytokines or factors regulating pericyte response (37). Recombinant Ang-2 did not affect alone the migration of control pericytes, as previously shown (37). However, recombinant Ang-2 significantly reduced the increased pericyte migration towards the supernatants of Ang-2-depleted ECs (Fig. 6D) or N6L-treated ECs (Fig 6E). Together these data demonstrate the crucial involvement of Ang-2 in the pro-normalizing effect induced by N6L.

N6L enhances drug delivery in PDAC treatment.

It has been shown that tumor vessel normalization represents a remarkably advantageous anti-cancer strategy, being also able to enhance drug delivery and, consequently, chemotherapy efficacy (23). To first assess whether the enhanced perfusion induced by N6L could also increase drug delivery, doxorubicin was injected in the tail vein of control or N6L-treated mice at the end of the trial and the amount of drug present into the tumor tissues was quantified. In line with the normalized vessel phenotype, N6L treatment increased by 3.5 times the efficacy of the doxorubicin delivery to the tumors of mPDAC, compared to controls (Fig. 7A). The resistance of PDAC tumors to chemotherapies, and consequently the extremely bad prognosis for PDAC patients is at least partly due to the extremely poor perfusion of blood vessels and drug delivery (38, 39). Increasing drug delivery represents a key strategy to treat PDAC patients. To evaluate whether the effect observed in mouse tumors was also observed in human cancers, both human BxPC-3-derived orthotopic (Fig. 7B) and

subcutaneous (Supplementary Fig. 5H) xenograft tumors were treated with N6L and doxorubicin was injected and quantified at the end of the treatment. N6L-treatment significantly increased the delivery of the drug into the tumor similarly to the mPDAC (Fig. 7B and Supplementary Fig. 5H). The time course of N6L treatment necessary to increase doxorubicin delivery induced by N6L was evaluated by a treatment of one or two weeks in subcutaneous BxPC-3 (Supplementary Fig. 5H). The improvement of the doxorubicin delivery by N6L was clearly improved by kinetics between the first and the second week of treatment (Supplementary Fig. 5H). Stemming from these data we sought to investigate whether the pre-treatment of N6L was able to enhance the anti-tumor effect of gemcitabine, the standard of care for PDAC human patients. Our preliminary data in mPDAC showed that the dose of 2 mg/kg N6L impaired tumor growth with less efficacy compared to the dose of 10 mg/kg, but was still able to induce pericyte coverage of tumor vessels (Fig 7C and Supplementary Fig. 4A). This suboptimal anti-tumor dose was therefore used to test the effects of the combination of N6L and gemcitabine in mPDAC model. Gemcitabine and N6L used as single agents had a similar effect in reducing tumor growth. Remarkably, the pre-treatment of mPDAC with N6L and the subsequent treatment with the combination of N6L with gemcitabine showed a greater effect in decreasing tumor volume in mPDAC, by 75% compared to the single treatments and by 82% compared to the control (Fig. 7C).

DISCUSSION

NCL inhibition is known to reduce tumor growth, and different strategies of NCL-targeted therapy are in development for clinical application in renal cell cancer and breast cancer (10, 11). In this study we described for the first time NCL-targeted therapy in pancreatic cancer. We used a highly aggressive and invasive orthotopic mouse PDAC model and RIP-Tag2 transgenic mouse model and demonstrated the antitumoral and anti-metastatic potential of the

N6L pseudopeptide on pancreatic cancer. Besides the effect of NCL on tumor cell proliferation, N6L targets also the tumor microenvironment reducing blood vessel area and promoting tumor vessel normalization that, in turn, impairs hypoxia and improves drug delivery.

PDAC is one of the most lethal cancers. The analysis of PDAC from human patients reveals that 74.5% of patients have a higher NCL level when compared with non-tumoral tissues. Importantly low level of NCL in PDAC correlates with increased survival of patients and may be a good prognostic factor. N6L exerts a potent anti-tumor and anti-metastatic effect in mPDAC, by inhibiting tumor proliferation and invasion, and inducing tumor apoptosis as previously described in breast and prostate xenograft tumors (9, 40). Conversely, since the complete knock down of Ncl in cells and adult animals was not viable, the side effects of NCL inhibition by a target therapy have to be carefully verified. The dose of N6L was recommanded by the results of the clinical trial phase I. NCL expression is regulated by cell proliferation (10) and the anti-proliferative activity of N6L was accompanied by a decrease of 50% of NCL expression in PDAC tumors.

Together, these findings, along with the OS observed in patients with low NCL level, suggest that the down-modulation of NCL levels in human patient by N6L treatment could contribute to the improvement of the survival in patients with pancreatic cancer.

Importantly, in PDAC, N6L induced tumor vessel normalization improving vessel perfusion and drug delivery. In addition, N6L efficiently affected tumor growth and tumor vasculature in RIP-Tag2, a mouse model highly vascularized in which anti-angiogenic therapies and vessel normalization has been demonstrated to be an efficient strategy to inhibit tumor growth (20). The strong effect of N6L on vessel normalization also in this model that displays a different angiogenic pattern compared to PDAC, further corroborates the selective effect of NCL inhibition on tumor stroma in pancreatic cancer. To further understand the importance of

NCL inhibition in the tumor vessel compartment, cancer vascularization was studied in a model of orthotopic PDAC developed in $Ncl^{+/+}$ or $Ncl^{+/-}$ background. This approach allowed us to clearly show that the single allele deletion of the stromal NCL is sufficient to impact the tumor vascularization, and that the tumor vessel normalization induced by NCL inhibition is not a secondary effect due to a reduced tumoral cell proliferation.

NCL is a marker of angiogenic vessels (7) and our data support an autocrine effect of the NCL inhibition on ECs. During angiogenesis, EC activation induces loss-of-quiescence of ECs (33) and the secretion of pro-angiogenic molecules (33). NCL inhibition by N6L starts a program of EC loss-of-activation through the induction of EC quiescence and promotion of an anti-angiogenic balance. Indeed, based on our proteome assay, N6L decreased the level of secreted pro-angiogenic molecules (Ang-2, FGF-2, VEGF-C and IL1β) (41) (42, 43) while enhanced anti-angiogenic molecules (Thrombospondin-1, Pentraxin-3 and Platelet factor 4) (44-46). Between the molecules regulated by N6L, Ang-2 and PDGFβ regulate pericyte recruitment (34). Remarkably, Ang-2 plasma levels were significantly reduced after N6L treatment together with its expression in the tumors, while plasma PDGFβ and VEGFA mRNA levels did not change. In addition, we demonstrated that NCL is involved in maintaining an active basal secretion of Ang-2 regulated by Weibel and Palade body exocytosis in activated ECs *in vitro*. While short-term NCL inhibition decreases Ang-2 secretion in ECs, longer NCL inhibition decreased the expression of Ang-2. This last effect is probably associated to the induction of EC quiescence, because Ang-2 is only expressed *in vivo* in remodeling and activated vessels (28). It is known that the Angiopoietins/TIE2 system regulates vascular development and maturation (41). Ang-1 activates TIE2 receptor and promotes vessel stabilization, while Ang-2, produced by activated ECs, promotes angiogenesis by inducing blood vessel destabilization and sprouting (41). Ang-2 blockade induces tumor vessel stabilization, decreases angiogenesis and slows the growth of several

tumor models (28-32). Based on these observations, we can argue that the observed pro-normalizing effect of N6L on tumor vasculature could be in part mediated by the inhibition of Ang-2 during the treatments. Notably, we observed that the depletion of Ang-2 and the inhibition of secretion by N6L in ECs are sufficient to promote pericyte migration. Since recombinant Ang-2 is able alone to rescue these effects, we could argue that the regulation of Ang-2 expression and secretion by ECs is crucial for pericyte recruitment. These findings suggest that the arrest of the EC cell cycle, along with the reduction of Ang-2 level *in vivo*, could contribute to the anti-angiogenic and pro-normalizing effect of NCL inhibition observed in mPDAC and RIP-Tag2 mice.

Single-agent gemcitabine is the standard-of-care treatment for PDAC patients, but the addition of targeted therapies to chemotherapy failed to show any improvement (47). One possible novel strategy to improve the current therapy in PDAC is to enhance drug delivery by targeting tumor microenvironment (39, 48, 49). However, decrease of PDAC solid stress by Shh deletion or Smoothened inhibition, increased vascular density, which in turn accelerated tumor growth and promoted metastasis (48). Interestingly, while the anti-angiogenesis therapies fail to improve PDAC survival, VEGFR inhibition was capable to counteract tumor angiogenesis induced by reduction of stroma stiffness (48). There is a growing body of evidences highlighting, both in pre-clinical and clinical settings, the importance of tumor vessel normalization, described by Jain and colleagues (23, 50). It has been demonstrated that the strong reduction of tumor hypoxia and the enhancement of vessel perfusion, accompanied by improved drug delivery, is a great advantage of using a pro-normalizing agent in anti-cancer therapies in the clinic (23). Remarkably, N6L treatment increased tumor vessel perfusion, strongly reduced tumor hypoxia and enhanced chemotherapeutic drug delivery *in vivo*. Consistently with the observed improved vessel perfusion and drug delivery to the tumor, pre-treatment of tumors with N6L strongly

enhanced the effect of gemcitabine on tumor growth in mPDAC. Further experiments will be needed to better assess the combinatorial effects of N6L and chemotherapeutic treatments on metastasis.

In conclusion, this work highlights a new therapeutic strategy that selectively targets NCL by dually targeting both cancer cells and tumor vessels in pancreatic cancer. We uncovered, for the first time, the inhibition of Ang-2 as a pro-normalizing mechanism of NCL-inhibition and important biomarker of N6L treatment. N6L treatment represents a new and more efficient anti-tumor and anti-angiogenic therapy for PDAC and insulinoma and could represent a promising drug to design combination therapies with established anticancer drugs or stroma-targeting molecules.

ACKNOWLEDGMENTS

This work was supported by grants from the French charitable organisation "Ligue National contre le Cancer", the "ANR-14-LE16-OO23-NORMATHER" and Immupharma. Associazione Italiana per la Ricerca sul Cancro (AIRC) investigator grants IG (# 15645); MIUR 2010 VASCHETTO – 5X1000 2010 FPRC-ONLUS), Swiss National Science Foundation (SNSF), Sinergia Grant (# CRSII3 160742/1).

REFERENCES

1. Matsuoka T, and Yashiro M. Molecular targets for the treatment of pancreatic cancer: Clinical and experimental studies. World J Gastroenterol 2016;22:776-89.
2. Garrido-Laguna I, and Hidalgo M. Pancreatic cancer: from state-of-the-art treatments to promising novel therapies. Nat Rev Clin Oncol 2015;12:319-34.
3. Jayson GC, Kerbel R, Ellis LM, and Harris AL. Antiangiogenic therapy in oncology: current status and future directions. Lancet. 2016.
4. Berger CM, Gaume X, and Bouvet P. The roles of nucleolin subcellular localization in cancer. Biochimie 2015;113:78-85.
5. Destouches D, El Khoury D, Hamma-Kourbali Y, Krust B, Albanese P, Katsoris P, et al. Suppression of tumor growth and angiogenesis by a specific antagonist of the cell-surface expressed nucleolin. PLoS One 2008;3:e2518.

6. Hovanessian AG, Soundaramourty C, El Khoury D, Nondier I, Svab J, and Krust B. Surface expressed nucleolin is constantly induced in tumor cells to mediate calcium-dependent ligand internalization. PLoS One 2011;5:e15787.
7. Christian S, Pilch J, Akerman ME, Porkka K, Laakkonen P, and Ruoslahti E. Nucleolin expressed at the cell surface is a marker of endothelial cells in angiogenic blood vessels. J Cell Biol 2003;163:871-8.
8. Otake Y, Soundararajan S, Sengupta TK, Kio EA, Smith JC, Pineda-Roman M, et al. Overexpression of nucleolin in chronic lymphocytic leukemia cells induces stabilization of bcl2 mRNA. Blood 2007;109:3069-75.
9. Destouches D, Page N, Hamma-Kourbali Y, Machi V, Chaloin O, Frechault S, et al. A simple approach to cancer therapy afforded by multivalent pseudopeptides that target cell-surface nucleoproteins. Cancer Res 2011;71:3296-305.
10. Bates PJ, Laber DA, Miller DM, Thomas SD, and Trent JO. Discovery and development of the G-rich oligonucleotide AS1411 as a novel treatment for cancer. Exp Mol Pathol 2009;86:151-64.
11. Pichiorri F, Palmieri D, De Luca L, Consiglio J, You J, Rocci A, et al. In vivo NCL targeting affects breast cancer aggressiveness through miRNA regulation. J Exp Med 2013;210:951-68.
12. Fogal V, Sugahara KN, Ruoslahti E, and Christian S. Cell surface nucleolin antagonist causes endothelial cell apoptosis and normalization of tumor vasculature. Angiogenesis 2009;12:91-100.
13. Birmpas C, Briand JP, Courty J, and Katsoris P. Nucleolin mediates the antiangiogenesis effect of the pseudopeptide N6L. BMC Cell Biol 2012;13:32.
14. Itakura J, Ishiwata T, Shen B, Kornmann M, and Korc M. Concomitant over-expression of vascular endothelial growth factor and its receptors in pancreatic cancer. Int J Cancer 2000;85:27-34.
15. Schulz P, Fischer C, Detjen KM, Rieke S, Hilfenhaus G, von Marschall Z, et al. Angiopoietin-2 drives lymphatic metastasis of pancreatic cancer. FASEB J 2011;25:3325-35.
16. Feig C, Gopinathan A, Neesse A, Chan DS, Cook N, and Tuveson DA. The pancreas cancer microenvironment. Clin Cancer Res 2012;18:4266-76.
17. Hanahan D, and Weinberg RA. Hallmarks of cancer: the next generation. Cell 2011;144:646-74.
18. Stylianopoulos T, and Jain RK. Combining two strategies to improve perfusion and drug delivery in solid tumors. Proc Natl Acad Sci U S A 2013;110:18632-7.
19. Hanahan D. Heritable formation of pancreatic beta-cell tumours in transgenic mice expressing recombinant insulin/simian virus 40 oncogenes. Nature 1985;315:115-22.
20. Maione F, Capano S, Regano D, Zentilin L, Giacca M, Casanovas O, et al. Semaphorin 3A overcomes cancer hypoxia and metastatic dissemination induced by antiangiogenic treatment in mice. J Clin Invest 2012;122:1832-48.
21. Hruban RH, Adsay NV, Albores-Saavedra J, Anver MR, Biankin AV, Boivin GP, et al. Pathology of genetically engineered mouse models of pancreatic exocrine cancer: consensus report and recommendations. Cancer Res 2006;66:95-106.
22. Gore J, Craven KE, Wilson JL, Cote GA, Cheng M, Nguyen HV, et al. TCGA data and patient-derived orthotopic xenografts highlight pancreatic cancer-associated angiogenesis. Oncotarget 2015;6:7504-21.
23. Jain RK. Antiangiogenesis strategies revisited: from starving tumors to alleviating hypoxia. Cancer Cell 2014;26:605-22.

24. Maione F, Molla F, Meda C, Latini R, Zentilin L, Giacca M, et al. Semaphorin 3A is an endogenous angiogenesis inhibitor that blocks tumor growth and normalizes tumor vasculature in transgenic mouse models. J Clin Invest 2009;119:3356-72.
25. Jain RK, Martin JD, and Stylianopoulos T. The role of mechanical forces in tumor growth and therapy. Annu Rev Biomed Eng 2014;16:321-46.
26. Beasley NJ, Wykoff CC, Watson PH, Leek R, Turley H, Gatter K, et al. Carbonic anhydrase IX, an endogenous hypoxia marker, expression in head and neck squamous cell carcinoma and its relationship to hypoxia, necrosis, and microvessel density. Cancer Res 2001;61:5262-7.
27. Cines DB, Pollak ES, Buck CA, Loscalzo J, Zimmerman GA, McEver RP, et al. Endothelial cells in physiology and in the pathophysiology of vascular disorders. Blood 1998;91:3527-61.
28. Maisonpierre PC, Suri C, Jones PF, Bartunkova S, Wiegand SJ, Radziejewski C, et al. Angiopoietin-2, a natural antagonist for Tie2 that disrupts in vivo angiogenesis. Science 1997;277:55-60.
29. Hammes HP, Lin J, Wagner P, Feng Y, Vom Hagen F, Krzizok T, et al. Angiopoietin-2 causes pericyte dropout in the normal retina: evidence for involvement in diabetic retinopathy Diabetes. 2004;53:1104-10.
30. Mazzieri R, Pucci F, Moi D, Zonari E, Ranghetti A, Berti A, et al. Targeting the ANG2/TIE2 axis inhibits tumor growth and metastasis by impairing angiogenesis and disabling rebounds of proangiogenic myeloid cells. Cancer Cell 2011;19:512-26.
31. Keskin D, Kim J, Cooke VG, Wu CC, Sugimoto H, Gu C, et al. Targeting vascular pericytes in hypoxic tumors increases lung metastasis via angiopoietin-2 Cell Rep. 2015;10:1066-81.
32. Srivastava K, Hu J, Korn C, Savant S, Teichert M, Kapel SS, et al. Postsurgical adjuvant tumor therapy by combining anti-angiopoietin-2 and metronomic chemotherapy limits metastatic growth. Cancer Cell 2014;26:880-95.
33. Fiedler U, and Augustin HG. Angiopoietins: a link between angiogenesis and inflammation. Trends Immunol 2006;27:552-8.
34. Abramsson A, Lindblom P, and Betsholtz C. Endothelial and nonendothelial sources of PDGF-B regulate pericyte recruitment and influence vascular pattern formation in tumors. J Clin Invest 2003;112:1142-51.
35. Audero E, Cascone I, Zanon I, Previtali SC, Piva R, Schiffer D, et al. Expression of angiopoietin-1 in human glioblastomas regulates tumor-induced angiogenesis: in vivo and in vitro studies. Arterioscler Thromb Vasc Biol 2001;21:536-41.
36. Sfiligoi C, de Luca A, Cascone I, Sorbello V, Fuso L, Ponzone R, et al. Angiopoietin-2 expression in breast cancer correlates with lymph node invasion and short survival. Int J Cancer 2003;103:466-74.
37. Cai J, Kehoe O, Smith GM, Hykin P, and Boulton ME. The angiopoietin/Tie-2 system regulates pericyte survival and recruitment in diabetic retinopathy. Invest Ophthalmol Vis Sci 2008;49:2163-71.
38. Koay EJ, Truty MJ, Cristini V, Thomas RM, Chen R, Chatterjee D, et al. Transport properties of pancreatic cancer describe gemcitabine delivery and response. J Clin Invest 2014;124:1525-36.
39. Olive KP, Jacobetz MA, Davidson CJ, Gopinathan A, McIntyre D, Honess D, et al. Inhibition of Hedgehog signaling enhances delivery of chemotherapy in a mouse model of pancreatic cancer. Science 2009;324:1457-61.
40. Destouches D, Sader M, Terry S, Marchand C, Maille P, Soyeux P, et al. Implication of NPM1 phosphorylation and preclinical evaluation of the nucleoprotein antagonist N6L in prostate cancer Oncotarget. 2016.

41. Augustin HG, Koh GY, Thurston G, and Alitalo K. Control of vascular morphogenesis and homeostasis through the angiopoietin-Tie system. Nat Rev Mol Cell Biol 2009;10:165-77.
42. Casanovas O, Hicklin DJ, Bergers G, and Hanahan D. Drug resistance by evasion of antiangiogenic targeting of VEGF signaling in late-stage pancreatic islet tumors. Cancer Cell 2005;8:299-309.
43. Shchors K, Shchors E, Rostker F, Lawlor ER, Brown-Swigart L, and Evan GI. The Myc-dependent angiogenic switch in tumors is mediated by interleukin 1beta. Genes Dev 2006;20:2527-38.
44. Dawson DW, Pearce SF, Zhong R, Silverstein RL, Frazier WA, and Bouck NP. CD36 mediates the In vitro inhibitory effects of thrombospondin-1 on endothelial cells. J Cell Biol 1997;138:707-17.
45. Alessi P, Leali D, Camozzi M, Cantelmo A, Albini A, and Presta M. Anti-FGF2 approaches as a strategy to compensate resistance to anti-VEGF therapy: long-pentraxin 3 as a novel antiangiogenic FGF2-antagonist. Eur Cytokine Netw 2009;20:225-34.
46. Perollet C, Han ZC, Savona C, Caen JP, and Bikfalvi A. Platelet factor 4 modulates fibroblast growth factor 2 (FGF-2) activity and inhibits FGF-2 dimerization. Blood 1998;91:3289-99.
47. Garrido-Laguna I, and Hidalgo M. Pancreatic cancer: from state-of-the-art treatments to promising novel therapies. Nat Rev Clin Oncol12:319-34.
48. Rhim AD, Oberstein PE, Thomas DH, Mirek ET, Palermo CF, Sastra SA, et al. Stromal elements act to restrain, rather than support, pancreatic ductal adenocarcinoma. Cancer Cell 2014;25:735-47.
49. Jacobetz MA, Chan DS, Neesse A, Bapiro TE, Cook N, Frese KK, et al. Hyaluronan impairs vascular function and drug delivery in a mouse model of pancreatic cancer. Gut 2012;62:112-20.
50. Serini G, Bussolino F, Maione F, and Giraudo E. Class 3 semaphorins: physiological vascular normalizing agents for anti-cancer therapy. J Intern Med. 2013;273:138-55.

FIGURE LEGENDS

Figure 1. NCL is highly expressed in human and PDAC mouse model.

Human PDAC included in a TMA were immunostained with anti-NCL antibody and scored as high (**A**), (**B**), moderate (**C**), low (**D**) or negative (see Methods). The NCL expression was barely detected in the tumor stroma and the surrounding pancreatitis (**D**). NCL was highly expressed by tumor glands (arrows in **A** and **B**) but not in normal ducts included in the tumor (arrowheads in **B**). (**E**) Kaplan–Meier overall survival (OS) curves (Mantel Cox Test, *p<0,0158).

Figure 2. N6L reduces PDAC tumor growth and liver metastasis.

Immunocompetent syngenic FVB/n mice were injected with mPDAC cells into the pancreas. Mice were treated one week after inoculation of tumor cells with N6L alone (10 mg/kg) or saline solution by i.p. 3 times a week for 3 weeks. Mice were sacrificed and tumor volumes were measured (**A**) (Student *t*-test, **P<0.01; n=10 mice). mPDAC tissues were immunostained with anti-Ki67 (**B**) or anti-active caspase 3 or NCL antibodies, and images show representative fields. White scale bars: 10 μm; black scale bar: 100 μm. The quantification of % of $Ki67^+$ cells (**C**) and of apoptotic cells (**D**) or NCL staining (**E**) were plotted as inhibition relative to control and were performed by ImageJ analysis as described in Methods (Student *t*-test, **P<0.01 *P<0.05, n=8 mice). (**F**) NCL mRNA level of PDAC tissues were quantified by qPCR and normalized to the GAPDH mRNA level (Ct_{NCL}-Ct_{GAPDH}) (Student *t*-test, *P<0.05, n=5 mice). For easier interpretation, histograms represent the fold change relative to control mice, calculated from the $2^{-\Delta\Delta Ct}$. (**G**) Representative histological images of liver sections (H&E staining) showing metastatic foci marked by black arrows. Scale bar: 100 μm. (**H**) The area of liver nodules were quantified by digitized image analysis using ImageJ software and plotted as the metastatic liver fraction (Student *t*-test one-tail, *P<0.05, n=5 mice).

Figure 3. N6L normalizes tumor blood PDAC vessels and counteracts tumor hypoxia in mPDAC.

PDAC mice were treated or not with N6L for 3 weeks as in Figure 2. (**A**) Tumor sections were immunostained by an anti-MECA32 antibody to detect tumor blood vessels, or co-immunostained by the anti-MECA32 and anti-NG2 or anti-PDGFRβ antibodies for pericyte analysis. Scale bars: 10 μm. Tumor vessels and pericyte coverage analysis were performed as described in Methods. In (**B**), the tumor blood vessel density, and in (**C**) tumor vessel branching are plotted as the % of the inhibition to control tumors. In (**D**) $NG2^+$ and in (**E**)

PDGFR-β^+ pericyte coverage of vessels are represented. In (**G**) vessel perfusion was assessed by tail-injecting animals with FITC-lectin at the end of the treatment with N6L and quantified as % of perfused/total blood (n=6 mice, Student *t*-test ****P<0.0001), and in (**F**) images are representative of lectin-FITC signal. (**H**) Hypoxia analysis was detected with an antibody recognizing the pimonidazole adducts (arrows) in control or N6L-treated tumor tissues. The area positive for pimonidazole adducts was 60% in Control and 25% in N6L. Tumor sections were immunostained by an anti-CA9 antibody for hypoxia-induced protein analysis (**I**) and the CA9 fluorescence intensity was plotted as a percentage relative to the control (**L**). In (**B**), (**C**), (**D**), (**E**) and (**J**), from at least n=5 mice per stage (Student *t*-test, ***P<0.001; **P<0.01; *P<0.05).

Figure 4. N6L normalizes RIP-Tag2 tumor blood vessels and blocks tumor growth.

(**A**) Total tumor volume in 4-weeks treatment regression trial showed that the treatment with N6L reduced tumor burden by 40% compared with controls (Student *t*-test, **P<0.01; n=6 mice). Tumor sections were immunostained by anti-active caspase 3 antibody (**B**) or co-immunostained by the anti-MECA32 and anti-NG2 for pericyte analysis (**C**). Scale bars: 20 μm. Quantification of apoptotic staining, tumor blood vessel density, tumor vessel branching and pericyte coverage have been performed as in Figure 3 and shown in (**B**), (**D**), (**E**), (**F**), respectively. (Student *t*-test, ****P<0,0001; ***P<0.001; **P<0.01; *P<0.05, n=5 mice). (**H**) Vessel perfusion was assessed as in Figure 3 (n=4 mice, Student *t*-test **P<0.01), and in (**G**) images are representative of lectin-FITC signal.

Figure 5. NCL inhibition blocks cell cycle in G1/S and decreases Ang-2 secretion.

In (**A**) and (**B**), ECs were incubated with N6L for 24 hours or transfected with siControl or siNCL. Cell cycle progression was analyzed by BrdU incorporation and the % cells in each

phase (G1, S, G2/M) is shown in the graph. (**B**) Efficiency of siNCL is shown by immunoblotting analysis. In (**C**) and (**F**), supernatants of ECs treated by increasing concentrations of N6L for 5 hours or from siControl or siNCL transfected ECs were analyzed by ELISA. The concentration of Ang-2 was normalized to the whole protein amount of the corresponding cell lysates in the different treatment groups. (**D**) N6L-treated ECs for 5 hours were fixed and coimmunostained with an anti-Ang-2 and anti-vWF antibodies, the Ang-2 area of staining per cell is plotted in (**E**). Insets show colocalization between the two stainings. (Student *t*-test, ***P<0.001, **P<0.05, *P<0.01, n=3 independent experiments).

In (**G**) and (**H**), ECs treated by N6L at 10 µM or transfected by NCL siRNA were lysed and Western Blotting of Ang-2 in EC lysates are shown. In (**I**) Ang-2 mRNA level of ECs treated by N6L were quantified by qPCR and normalized to the GAPDH mRNA level, histograms represent the fold change relative to control cells (±SEM) of 3 independent experiments, calculated from the $2^{-\Delta\Delta Ct}$ (Student *t*-test, *P<0.05).

Figure 6. NCL inhibition decreases Ang-2 secretion by ECs and plasma Ang-2.

(**A**) FVB/n mice were injected with PDAC cells (PDAC) or saline solution (Control) into the pancreas, blood samples were collected after 3 weeks (W3) or (**B)** PDAC mice were treated or not with N6L for 3 weeks as in Figure 3 (W4). Plasma Ang-2 was quantified by ELISA (Student *t*-test, *P<0.05, n=6 mice). (**C)** Ang-2 mRNA level of PDAC tissues were quantified by qPCR and normalized to the MECA32 mRNA level ($Ct_{Ang\text{-}2}$-Ct_{MECA32}) (n=5 mice, Student *t*-test, *P<0.05). For easier interpretation, histograms represent the fold change relative to Control mice, calculated from the $2^{-\Delta\Delta Ct}$. (**D**) and (**E**) HBVP were allowed to migrate in the presence of supernatants of siControl- or siAng2-transfected or N6L-treated ECs. Recombinant Ang-2 at 100 ng/ml was added as indicated. The graph shows the fold increase of pericyte migration relative to control cells (Student *t*-test, *P<0.01, *P<0.05, n=3

experiments). On the right, immunoblotting analysis of Ang-2 in siControl or siAng2-transfected ECs, Ang-2 depletion was of 90% by siRNA transfection.

Figure 7. NCL inhibition improves drug delivery to the tumor.

Doxorubicin delivery was evaluated after 3 weeks of treatment of PDAC-carrying animals with N6L (**A**) or 2 weeks of treatment of BxPC-3 orthotopic tumors (**B**). Amount of doxorubicin (DXR) present in tumors was expressed as μg equivalent/g tumor. N6L enhanced doxorubicin delivery to PDAC 3.5 fold and 1.9 fold to BxPC-3. (Student *t*-test, *P<0.05, n=6 mice). (**C**) Immuno-competent syngenic FVB/n mice were injected with PDAC cells into the pancreas, and treated with control and N6L, alone or in combination with gemcitabine (GEM. Mice were sacrificed and tumor volumes were measured (Student *t*-test, ****P<0.0001, ***P<0.001, **P<0.01; control n=5, N6L n=4, gemcitabine n=7, N6L+GEM n=7).

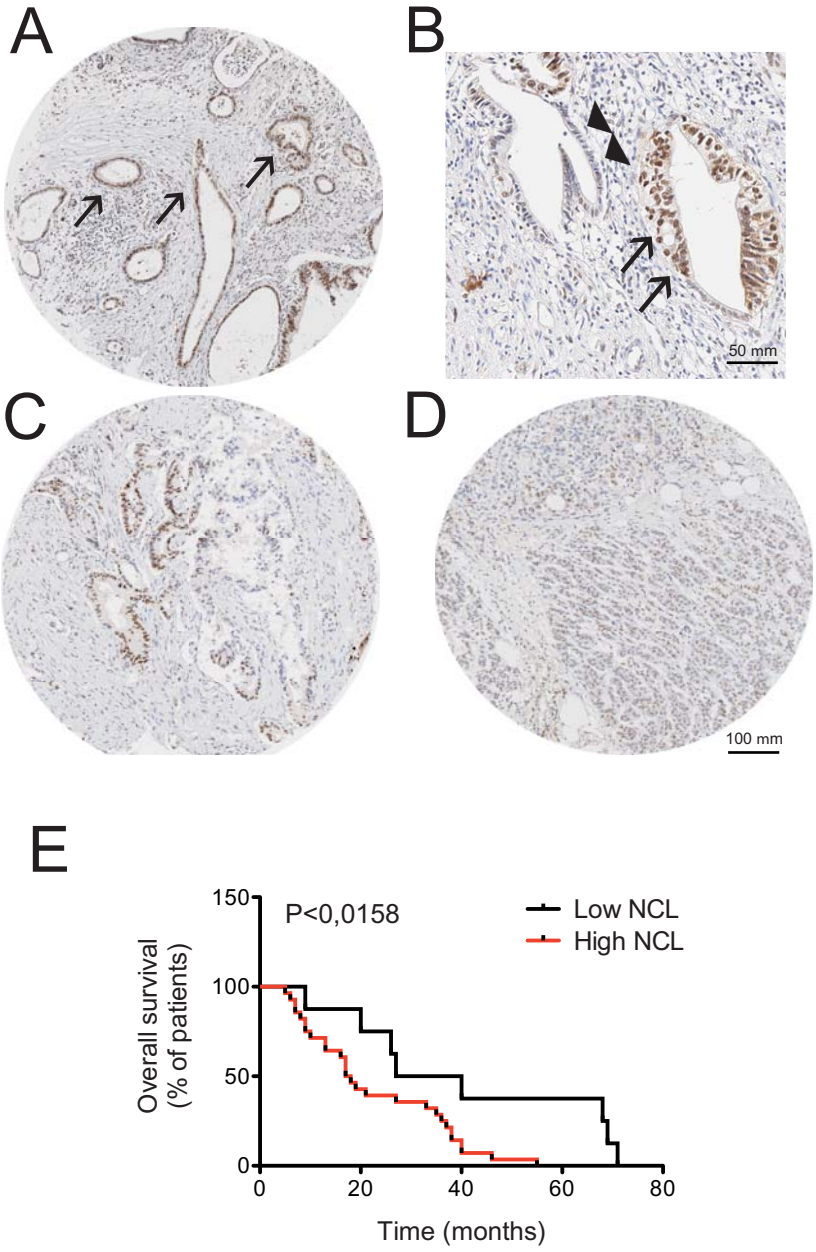
A
B
50 mm
C
D
100 mm
E
P<0,0158
Low NCL
High NCL
Overall survival
(% of patients)
150
100
50
0
0
20
40
60
80
Time (months)

Figure 1

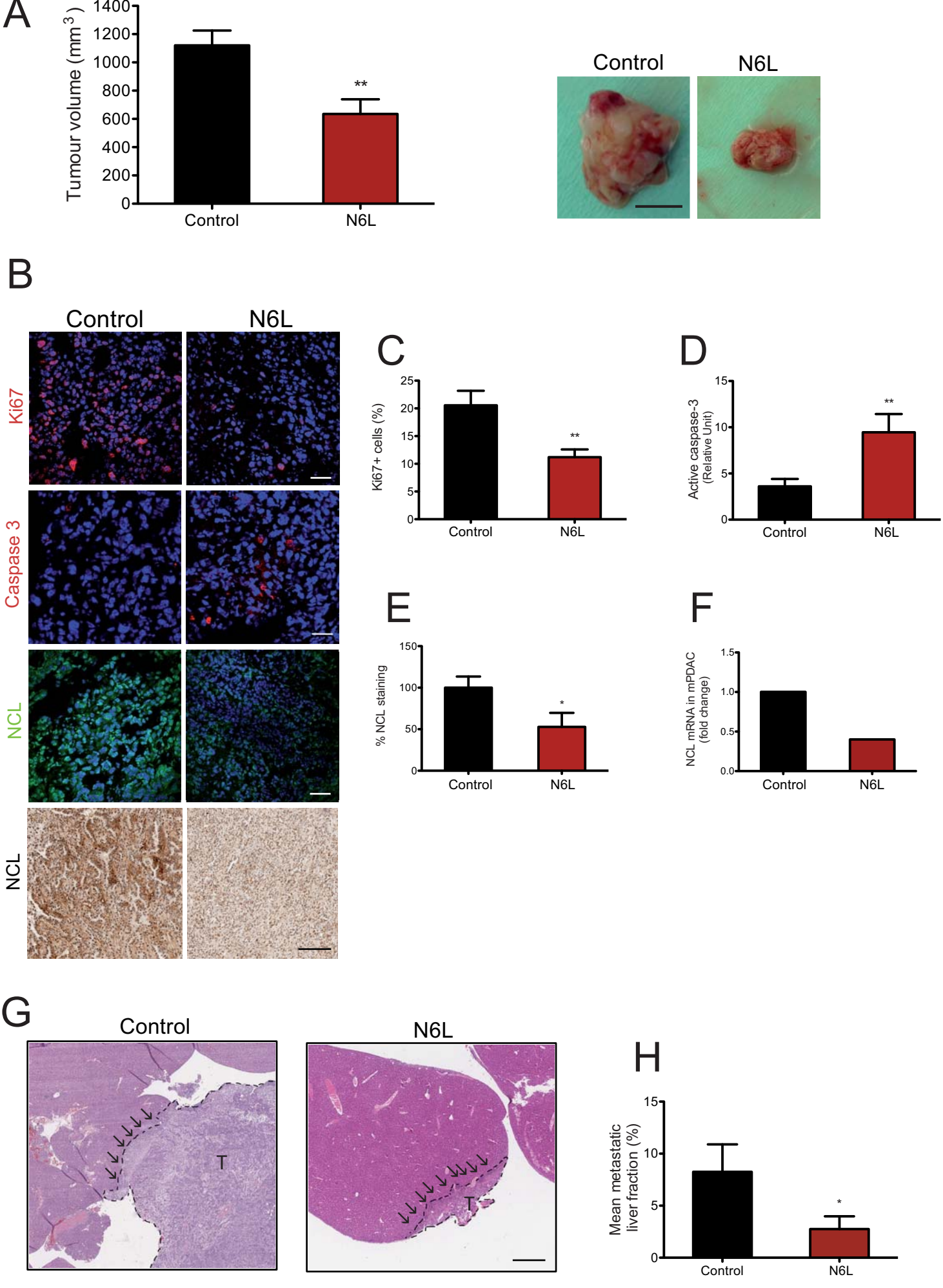
A
Tumour volume (mm3)
1400
1200
1000
800
600
400
200
0
**
Control
N6L
Control
N6L
B
Control
N6L
Ki67
Active Caspase 3
NCL
NCL
C
Ki67+ cells (%)
25
20
15
10
5
0
**
Control
N6L
D
Active caspase-3 (Relative Unit)
15
10
5
0
**
Control
N6L
E
% NCL staining
150
100
50
0
*
Control
N6L
F
NCL mRNA in mPDAC (fold change)
1.5
1.0
0.5
0.0
Control
N6L
G
Control
N6L
T
T
H
Mean metastatic liver fraction (%)
15
10
5
0
*
Control
N6L

Figure 2

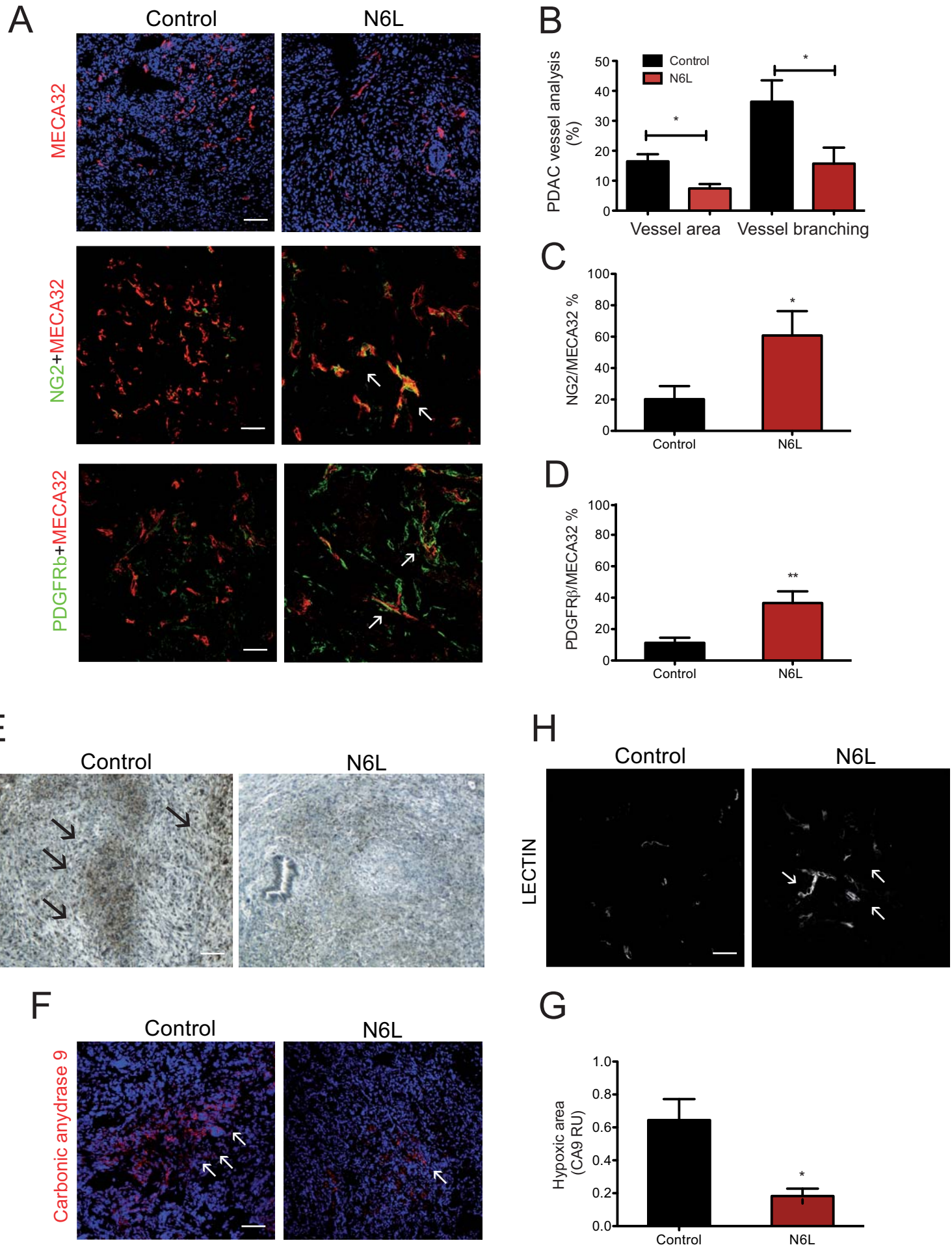
A
Control
N6L
MECA32
NG2+MECA32
PDGFRb+MECA32
B
PDAC vessel analysis (%)
Control
N6L
Vessel area
Vessel branching
C
NG2/MECA32 %
Control
N6L
D
PDGFRβ/MECA32 %
Control
N6L
E
Control
N6L
Pimonidazole
F
Control
N6L
Carbonic anydrase 9
G
Hypoxic area (CA9 RU)
Control
N6L
H
Control
N6L
LECTIN

Figure 3

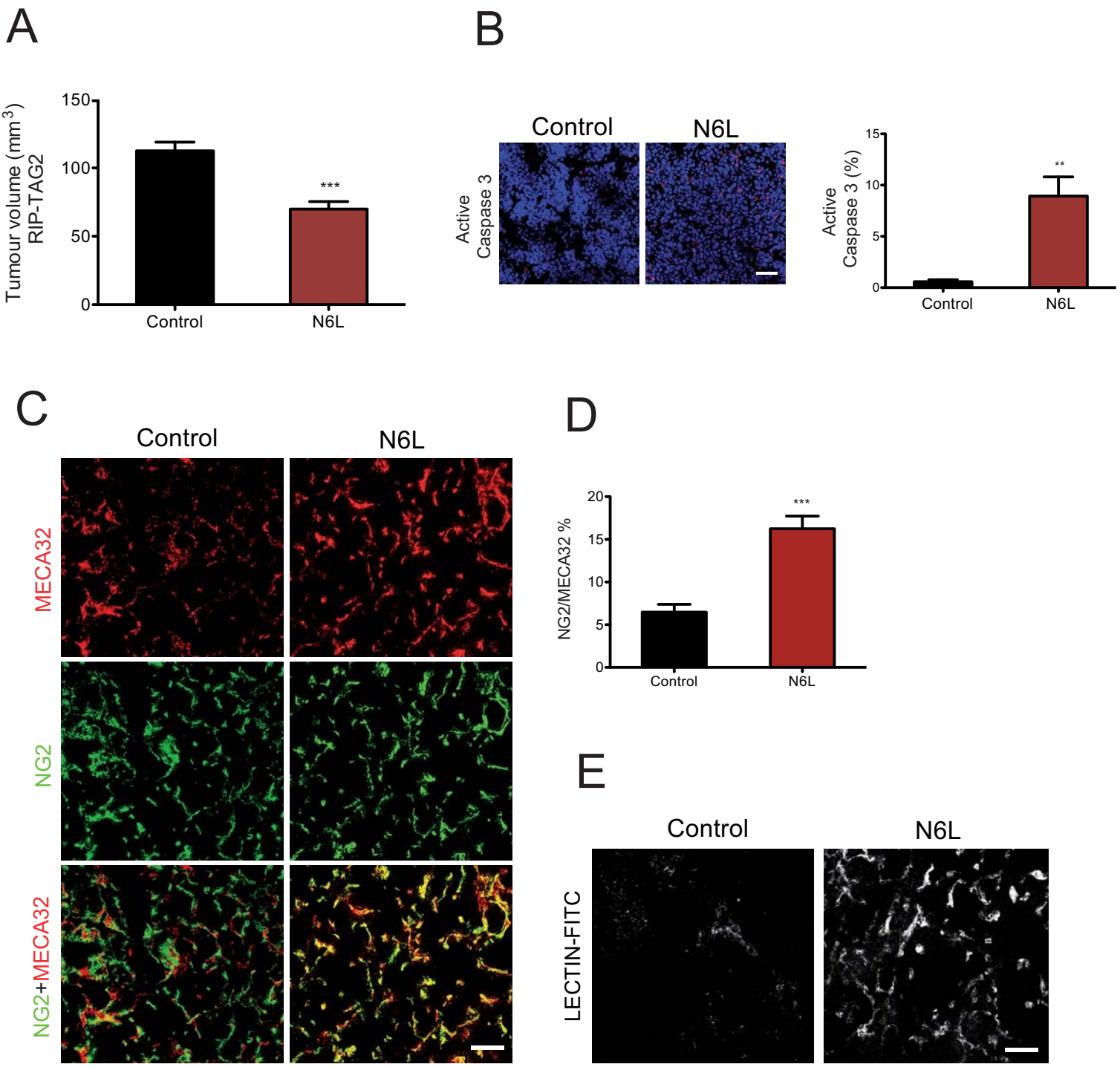
A
Tumour volume (mm3)
RIP-TAG2
150
100
50
0
***
Control
N6L
B
Control
N6L
Active
Caspase 3
Active
Caspase 3 (%)
15
10
5
0
**
Control
N6L
C
Control
N6L
MECA32
NG2
NG2+MECA32
D
NG2/MECA32 %
20
15
10
5
0
***
Control
N6L
E
Control
N6L
LECTIN-FITC

Figure 4

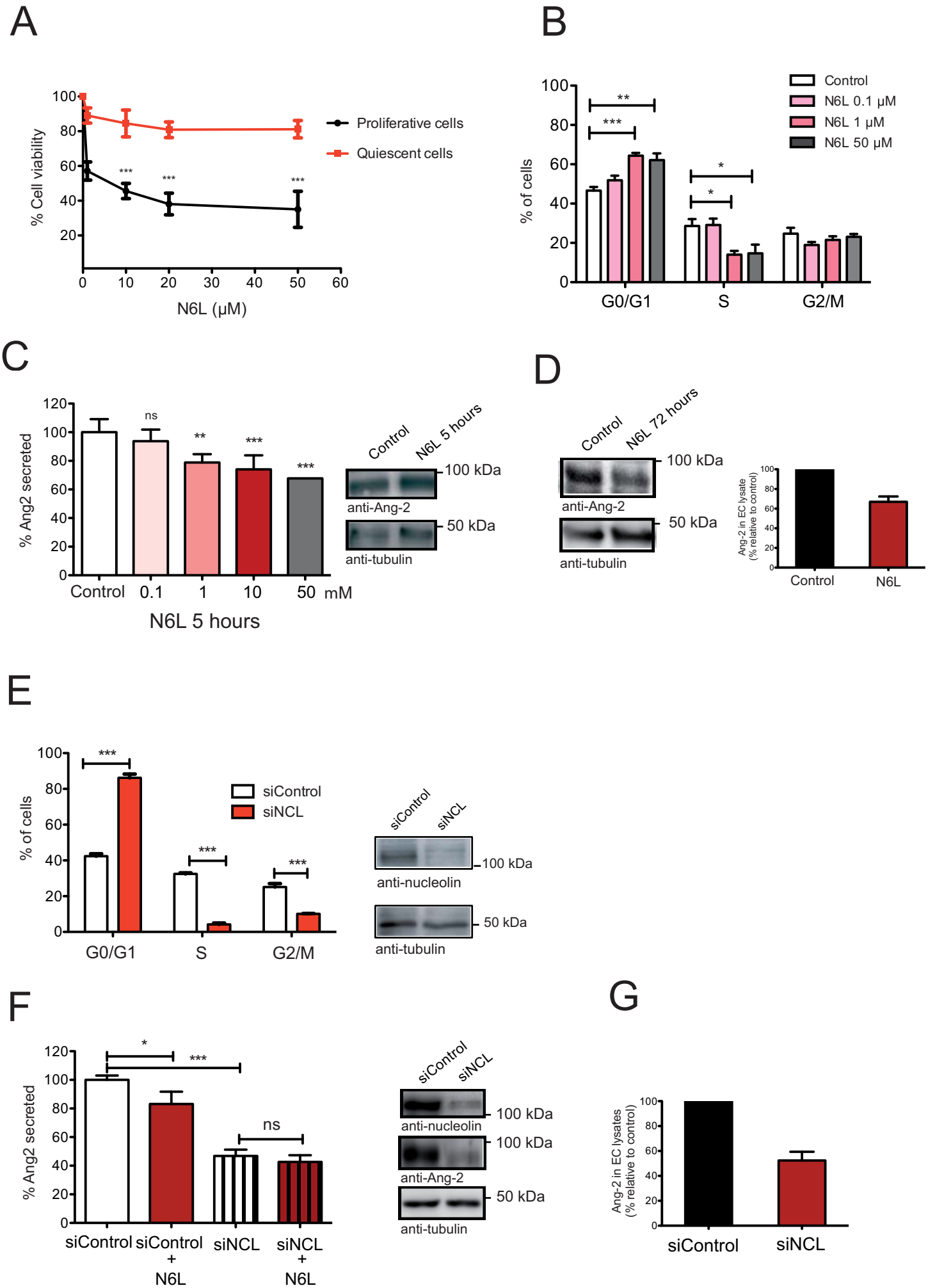
A
% Cell viability
N6L (μM)
Proliferative cells
Quiescent cells
B
% of cells
Control
N6L 0.1 μM
N6L 1 μM
N6L 50 μM
G0/G1
S
G2/M
C
% Ang2 secreted
Control
0.1
1
10
50 mM
N6L 5 hours
ns
Control
N6L 5 hours
100 kDa
anti-Ang-2
50 kDa
anti-tubulin
D
Control
N6L 72 hours
100 kDa
anti-Ang-2
50 kDa
anti-tubulin
Ang-2 in EC lysate (% relative to control)
Control
N6L
E
% of cells
siControl
siNCL
G0/G1
S
G2/M
siControl
siNCL
100 kDa
anti-nucleolin
50 kDa
anti-tubulin
F
% Ang2 secreted
siControl
siControl + N6L
siNCL
siNCL + N6L
ns
siControl
siNCL
100 kDa
anti-nucleolin
100 kDa
anti-Ang-2
50 kDa
anti-tubulin
G
Ang-2 in EC lysates (% relative to control)
siControl
siNCL

Figure 5

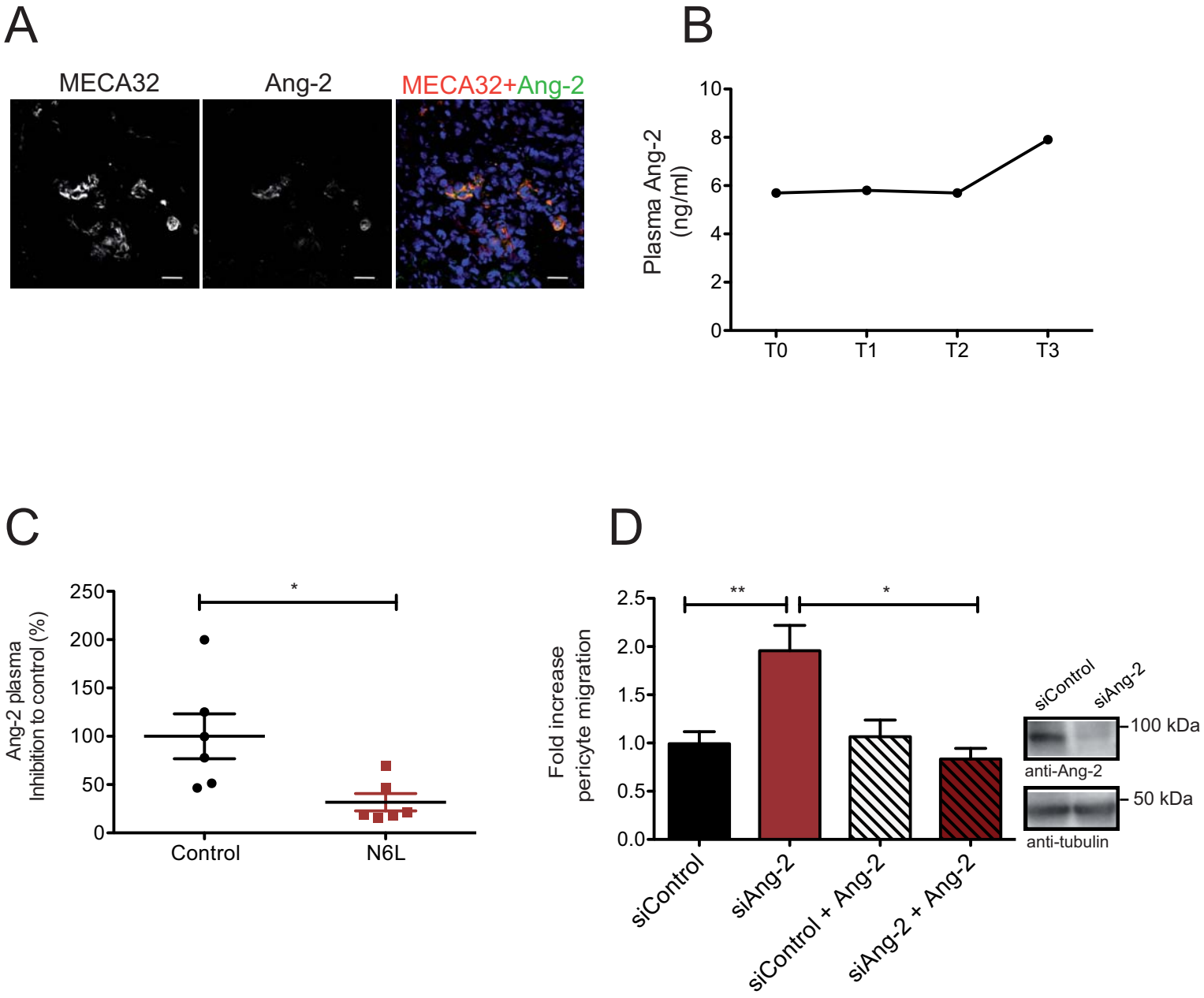
A
MECA32
Ang-2
MECA32+Ang-2
B
Plasma Ang-2 (ng/ml)
10
8
6
4
2
0
T0
T1
T2
T3
C
Ang-2 plasma Inhibition to control (%)
250
200
150
100
50
0
*
Control
N6L
D
Fold increase pericyte migration
2.5
2.0
1.5
1.0
0.5
0.0
**
*
siControl
siAng-2
siControl + Ang-2
siAng-2 + Ang-2
siControl
siAng-2
100 kDa
anti-Ang-2
50 kDa
anti-tubulin

Figure 6

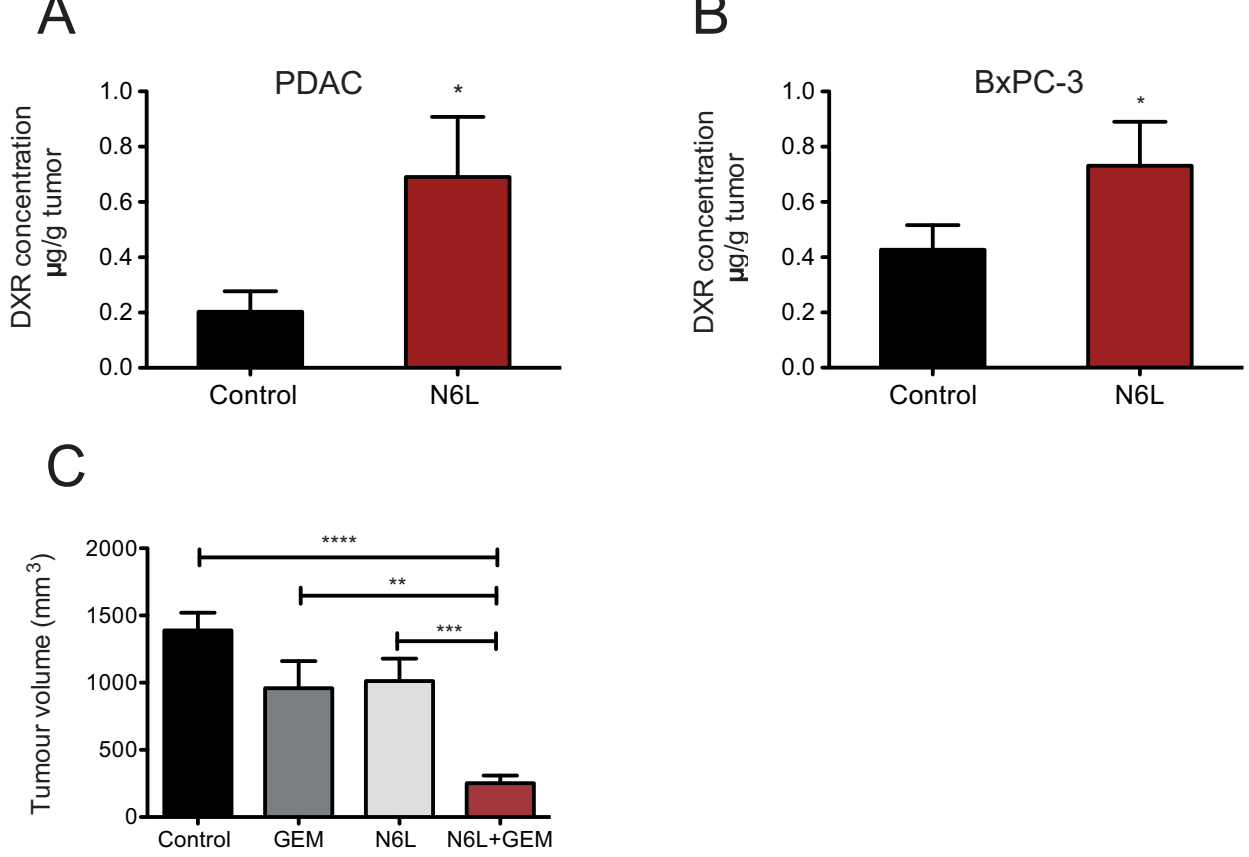
A
PDAC
DXR concentration µg/g tumor
1.0
0.8
0.6
0.4
0.2
0.0
*
Control
N6L
B
BxPC-3
DXR concentration µg/g tumor
1.0
0.8
0.6
0.4
0.2
0.0
*
Control
N6L

C
Tumour volume (mm3)
2000
1500
1000
500
0
****
**
***
Control
GEM
N6L
N6L+GEM

Figure 7